The Astrophysical Journal, 612:974–987, 2004 September 10

THE LATE-TIME RADIO EMISSION FROM SN 1993J AT METER WAVELENGTHS

P. Chandra
Tata Institute of Fundamental Research, Mumbai 400 005, India; and Joint Astronomy Programme, Indian Institute of Science, Bangalore 560 012, India; poonam@tifr.res.in

A. Ray
Tata Institute of Fundamental Research, Mumbai 400 005, India; akr@tifr.res.in

and

S. Bhatnagar
National Radio Astronomy Observatory, Socorro, NM 87801; sbhatnag@aoc.nrao.edu
Received 2003 December 19; accepted 2004 May 20

ABSTRACT

This paper presents the investigations of SN 1993J using low-frequency observations with the Giant Metrewave Radio Telescope (GMRT). We analyze the light curves of SN 1993J at 1420, 610, 325, and 243 MHz during 7.5–10 yr after the explosion. The supernova has become optically thin early on in the 1420 and 610 MHz bands, while it has only recently entered the optically thin phase in the 325 MHz band. The radio light curve in the 235 MHz band is more or less flat. This indicates that the supernova is undergoing a transition from an optically thick to optically thin limit in this frequency band. In addition, we analyze the supernova radio spectra at five epochs on days 3000, 3200, 3266, 3460, and 3730 after the explosion. The spectral break in the day 3200 composite spectrum from the GMRT and Very Large Array implies that the plasma is dominated by a magnetic field, and the latter is far from being in equipartition with relativistic particles. SN 1993J is the only young supernova for which the magnetic field and the size of the radio-emitting region are determined through unrelated methods. Thus, the mechanism that controls the evolution of the radio spectra can be identified. We suggest that at all epochs, the synchrotron self-absorption mechanism is primarily responsible for the turnover in the spectra. Light-curve models based on free-free absorption in homogeneous or inhomogeneous media at high frequencies overpredict the flux densities at low frequencies. The discrepancy is increasingly larger at lower and lower frequencies. We suggest that an extra opacity, sensitively dependent on frequency, is likely to account for the difference at lower frequencies. The evolution of the magnetic field (determined from synchrotron self-absorption turnover) is roughly consistent with $B \propto t^{-1}$. The radio spectral index in the optically thin part evolves from $\alpha \sim 0.8$–1.0 at a few tens of days to ~ 0.6 in about 10 yr.

Subject headings: circumstellar matter — radiation mechanisms: nonthermal — shock waves — stars: magnetic fields — stars: mass loss — supernovae: individual (SN 1993J)

1. INTRODUCTION

Supernova SN 1993J exploded on 1993 March 28 (Ripero et al. 1993) in the nearby galaxy M81 at a distance of 3.6 Mpc (Freedman et al. 1994). The early spectrum of SN 1993J showed the characteristic hydrogen-line signature of Type II supernovae but subsequently made a transition to a hydrogen-free, helium-dominated Type Ib supernova (Swartz et al. 1993; Filippenko et al. 1993). SN 1993J was therefore classified as an archetypal "Type IIb" supernova. The supernova provided a very good opportunity for a detailed study of extragalactic supernovae, first because it was one of the nearest extragalactic supernovae, and second because it was easily observable from the northern hemisphere for most of a year because of its high positive declination. It was extensively observed soon after its discovery in the nonoptical bands as well. The radio detection at 1.4 cm with the Very Large Array (VLA) took place on day 5 (Weiler et al. 1993), while in the X-ray bands, *ROSAT* detected it on day 6 (Zimmermann et al. 1993a, 1993b).

Optical observations of the pre- and postsupernova fields of SN 1993J indicated that its progenitor was an early K-type supergiant star with $M_V = -7.0 \pm 0.4$ mag and an initial mass of 13–22 $M_\odot$ (Van Dyk et al. 2002). The photometric evolution of SN 1993J indicated that it had very little hydrogen left in the outermost shell. This suggested that the progenitor was more likely a part of a binary system. The outermost hydrogen envelope of the progenitor was largely stripped off by the massive binary companion (Ray et al. 1993; Nomoto et al. 1993; Podsiadlowski et al. 1993; Woosley et al. 1994; Utrobin 1994). The possibility that it was a very massive Wolf-Rayet star ($\sim$30 $M_\odot$) that lost most of its outermost envelope before the explosion had also been advocated (Höflich et al. 1993). However, recent high-resolution photometric and spectroscopic observations of SN 1993J with the *Hubble Space Telescope*, 10 years after the explosion, have unambiguously detected the signature of a massive binary companion of SN 1993J with almost the same mass (14–15 $M_\odot$) as that of the progenitor (Maund et al. 2004).

Radio emission from supernovae is due to the interaction of the supernova ejecta with the circumstellar medium (CSM). CSM is created in the early evolutionary phases of a progenitor star from the mass loss from the star before it undergoes explosion. For supernova ejecta moving with supersonic speeds, interaction with the CSM gives rise to a low-density, high-temperature, forward-shocked shell and a high-density, low-temperature, reverse-shocked region. The radio emission is believed to be due to nonthermal electron synchrotron emission from the hydrodynamically unstable interaction region. This region contains shocked supernova ejecta, as well as swept-up circumstellar material separated by a contact discontinuity, and is bounded outward by the blast-wave shock

and inward by the reverse shock. The radio emission can be absorbed by the surrounding dense CSM through free-free absorption (FFA). It can also undergo synchrotron self-absorption (SSA) in the magnetized plasma. In general, light curves of supernovae show an initial smooth rise of radio flux density in their early stage because of decreasing absorption of the overlying medium and subsequently a smooth fall due to the decreasing density of the CSM. The optical depth of the FFA is defined as $\tau = \int k_{\rm ff}\, ds \propto R^{-3}\nu^{-2}$, and $k_{\rm ff}$ is the absorption coefficient, which depends on n_e and n_i, the electron and ion number densities, respectively. Since $n_e \propto R^{-2}$, $n_i = \overline{Z} n_e$, and the thermally averaged $k_{\rm ff} \propto \nu^{-2.1} T^{-1.35}$, the dependence of the optical depth on size and frequency is $\tau \propto R^{-3}\nu^{-2.1}$. The light curves show that the lower frequencies progressively become optically thin at later epochs, i.e., the radio emission peak shifts to lower frequencies with time. In some supernovae FFA is dominant, while in others SSA may become important depending on the mass-loss rate, shock velocity, and circumstellar temperature, etc. SSA is usually dominant in ejecta with high velocities and high CSM temperatures, whereas a high mass loss rate favors FFA mechanisms (Chevalier & Fransson 2003). For example, the light curves of SN 1979C fit well with an FFA model (Weiler et al. 1991), whereas the SN 1998bw evolution can be well described by an SSA model (Kulkarni et al. 1998). In some cases, the light curves exhibit nonsmooth behavior (e.g., a steep decline or a sharp jump in the flux density). This could be due to inhomogeneities in the CSM. The magnetic field in the shocked shell of a supernova, amplified by instabilities near the contact surface, may also have an inhomogeneous distribution.

Even though SN 1993J has been extensively observed at high radio frequencies, its evolution at low frequencies is critical at late epochs. We sampled the light curves of SN 1993J at lower frequencies between 7.5 and 10 yr after the explosion using the Giant Metrewave Radio Telescope (GMRT) at the 1420, 610, 325, and 235 MHz bands. We also obtained simultaneous to near-simultaneous spectra of the supernova on five occasions. On one occasion, we combined GMRT plus VLA data and obtained a wide-band radio spectrum. This composite spectrum around 3200 days shows evidence of synchrotron cooling. The implications of this result on the magnetic field and equipartition fraction in SN 1993J are published elsewhere (Chandra et al. 2004a). These results are used extensively in this paper. Our data also suggest that the turnover in the radio spectrum can be explained reasonably well by SSA. FFA appears to have a minor role compared to SSA in determining the spectral turnover at low frequencies. We note that the simple extrapolation of the FFA model obtained from high-frequency observations of SN 1993J fails to reproduce and overpredicts the observed flux densities at low frequencies. We discuss the evolution of the supernova's size, magnetic field, and radio spectral index with time, starting from a few tens of days to 3700 days after the explosion.

Section 2 gives the details of our observations and data analysis. We discuss in § 3 the light curves and spectra of SN 1993J at low frequencies. We also give our interpretations of the light curves and spectra in § 3. The summary and conclusions are given in § 4.

2. OBSERVATIONS AND DATA ANALYSIS

2.1. *GMRT Observations*

We observed SN 1993J with the GMRT on several occasions at multiple frequencies (1420, 610, 325, and 235 MHz). The monitoring program for SN 1993J was started in 2000 November and continued until 2003 June. We also obtained simultaneous to near-simultaneous spectra of the supernova on five occasions. The total time spent on the supernova during the observations at various epochs varied from 2 to 4 hr. About 17–29 good antennas could be used in the radio interferometric setup for flux density measurements of the supernova at different observing epochs. For the 1420, 610, and 325 MHz bands, the bandwidth used was 16 MHz (divided into a total of 128 frequency channels, the default for the GMRT correlator), while it was 6 MHz for the 243 MHz wave band. Table 1 gives the observing log for SN 1993J.

2.2. *Calibrators*

Calibrator sources were used to remove the effect of variation of the instrumental factors in the measurements. 3C 48 and 3C 147 were used as flux calibrators at 1420 MHz. At lower frequencies, i.e., the 610, 325, and 243 MHz bands, 3C 286, 3C 48, and 3C 147 were used as flux calibrators. The flux densities of the flux calibrators at the observing frequencies were derived using the Baars formulation (Baars et al. 1977). Table 2 lists the flux calibrators and their flux densities at all GMRT wave bands.

For the 1420 MHz observations, the source 1035+564 (J2000.0 coordinates: R.A. $= 10^{\rm h}35^{\rm m}07\overset{\rm s}{.}0$, decl. $= +56^\circ 28' 47''$) was used as a phase calibrator on all occasions, except for the 2000 November 8, 2000 December 16, and 2001 June 2 observations, when 0834+555 was used as the phase calibrator. For the 610, 325, and 235 MHz band observations, 0834+555 (J2000.0 coordinates: R.A. $= 08^{\rm h}34^{\rm m}54\overset{\rm s}{.}9$, decl. $= +55^\circ 34' 21''$) was used as a phase calibrator in all observations carried out by us. We used the flux calibrators and phase calibrators for bandpass calibration as well. Flux calibrators were observed once or twice for 20–30 minutes during each observing session. Phase calibrators were observed for 5–6 minutes after every 25 minutes of observation of the supernova. Observations of the phase calibrators separated by small time intervals were important not only for the tracking of instrumental phase and gain drifts and atmospheric and ionospheric gain and phase variations but also for monitoring the quality and sensitivity of the data and for spotting occasional gain and phase jumps. Table 3 gives the details of the observations of the phase calibrator 1035+564 at the 1420 MHz band on five occasions. Table 4 gives the details of the phase calibrator 0834+555 at all other occasions and in all the frequency bands.

Tables 3 and 4 give the positions of the phase calibrator obtained from GMRT observations and their offsets from the optical position of the source taken from the NASA Extragalactic Database (NED). We note that in earlier observations, the offset in the positions is sometimes significant. This is because until 2001 June, the GMRT antennas were pointing at the apparent positions of the sources (uncorrected for the effects due to nutation and aberration, etc.) and were not corrected to their mean positions. Thus, some of the observations gave large position offsets, sometimes as large as a few tens of arcseconds. However, we found in the cases in which the phase calibrators had large offsets from the optical positions that all sources in the supernova field of view were offset from their respective optical positions by the same amount.

2.3. *Data Analysis*

Data analysis at high frequencies is easier than that at lower frequencies. At high frequencies, the bandwidth smearing across the observing frequency band is negligible in contrast

TABLE 1
DETAILS OF THE GMRT OBSERVATIONS OF SN 1993J

Date of Observation	Days after Explosion	Frequency Band (MHz)	Number of Good Antennas	Resolution (arcsec)	Flux Density (mJy)	rms (mJy)
2000 Nov 8	2779	1420	19	25 × 18	35.1 ± 3.5	0.5
2000 Dec 16	2818	1420	23	8 × 5	36.1 ± 3.6	0.3
2001 Jun 2	2988	1390	28	4 × 3	32.7 ± 3.3	0.2
2001 Oct 15	3123	1390	24	10 × 6	33.9 ± 3.3	0.3
2002 Apr 7	3296	1390	25	11 × 7	24.6 ± 3.7	1.0
2002 Jun 24	3374	1390	19	6 × 3	23.4 ± 2.5	0.4
2002 Sep 21	3463	1390	25	5 × 3	24.2 ± 2.4	0.2
2003 Jun 13	3728	1280	24	5 × 2	20.2 ± 2.1	0.2
2001 Mar 24	2917	610	20	11 × 7	56.1 ± 5.5	0.5
2001 Aug 24	3072	610	24	13 × 7	55.8 ± 5.7	0.4
2001 Dec 30	3198	610	20	11 × 8	47.8 ± 5.5	1.9
2002 Mar 8	3266	610	25	14 × 6	44.4 ± 4.5	0.3
2002 May 19	3338	610	24	18 × 8	44.6 ± 4.5	0.6
2002 Sep 16	3458	610	26	10 × 6	37.5 ± 3.8	0.4
2003 Jun 17	3732	610	23	14 × 5	33.4 ± 4.3	0.8
2001 Jul 5	3022	325	18	19 × 10	69.2 ± 15.8	2.5
2002 Mar 7	3265	325	24	19 × 13	55.8 ± 7.4	1.9
2002 Aug 16	3427	325	16	18 × 9	61.8 ± 8.8	2.7
2001 Dec 31	3199	243	20	19 × 14	57.8 ± 7.6	2.5
2002 Mar 8	3266	243	17	26 × 16	60.9 ± 10.8	4.1
2002 Sep 16	3458	243	17	26 × 16	56.7 ± 8.7	4.0
2003 Jun 17	3732	243	22	23 × 11	58.2 ± 11.8	5.4

to the case for low frequencies. Bandwidth smearing occurs because of the averaging of visibilities over a finite bandwidth and is directly proportional to $\Delta\nu/\nu$. This is large at low frequencies and leads to significant smearing. One needs to divide the total bandwidth of observation, $\Delta\nu$, into subbands $\delta\nu_i$ so that $\delta\nu_i/\nu$ is small enough for insignificant smearing and then stack the subbands together, in order not to lose the sensitivity. At high frequencies, the w-term can be ignored, and a two-dimensional approximation of the sky is valid. At lower frequencies, however, this assumption breaks down. This is because at low frequencies, the antenna primary beam (λ/D, where λ is the wavelength of observation and D is the antenna diameter) is much too large to be approximated by a single tangent plane. Three-dimensional imaging is required, which is performed by dividing the whole field of view into multiple subfields and imaging each field separately. We find that for GMRT the minimum number of subfields required is 2, 6, 11, and 15 at the 1420, 610, 325, and 243 MHz frequency bands, respectively.[1]

[1] The number of planes required at a given wavelength λ is $N_{\rm planes} = \lambda B/D^2$, where B is the longest baseline separation (25 km for GMRT) and D is the antenna diameter (45 m for GMRT).

The Astrophysical Image Processing System (AIPS) developed by NRAO was used to analyze all data sets with the standard GMRT data reduction. Bad antennas and corrupted data were removed using standard AIPS routines. Data were then calibrated, and images of the fields were formed by Fourier inversion and cleaning using the AIPS task *imagr* (see Bhatnagar 2000, 2001 for details of the data analysis procedure). For the 1420 and 610 MHz data sets, bandwidth smearing effects were negligible, and imaging was done after averaging 100 central frequency channels (out of the total of 128 channels). For the 325 MHz analysis, the 96 central channels (12 MHz bandwidth) were divided into four subbands of 3 MHz each for imaging. For the 243 MHz analysis, we usually took 60–70 good central channels and divided them into four subbands for imaging. While making images, these subbands were stacked together. To take care of the wide-field imaging, we divided the whole field of view into two to five subfields for the 1420 MHz frequency data sets and into five to nine subfields for the 610 MHz data sets. For the 325 MHz data sets, wide-field imaging was performed with 16–25 subfields, while for the 245 MHz data sets, this was done with 25–36 subfields. We performed a few rounds of phase self-calibrations in all the data sets to remove the phase

TABLE 2
DETAILS OF THE FLUX CALIBRATORS USED

		Position (J2000.0)		Flux Density[a] (Jy)			
Name	Redshift	R.A.	Decl.	1420 MHz	610 MHz	325 MHz	235 MHz
3C 48	0.367	01 37 41.3	33 09 35	16.2	29.4	43.4	50.8
3C 147	0.545	05 42 36.1	49 51 07	22.3	38.3	52.7	59.2
3C 286	0.849	13 31 08.3	30 30 33	...	21.1	25.9	28.1

NOTE.—Units of right ascension are hours, minutes, and seconds, and units of declination are degrees, arcminutes, and arcseconds.
[a] The flux density of the flux calibrators were calculated using Baars formulation (Baars et al. 1977). Here it was assumed that these sources evolve as a single power law with respect to frequency, taken from the VLA calibrator catalog.

TABLE 3
GMRT Observations of the Phase Calibrator 1035+564 at the 1390 MHz Band

Date of Observation	Flux Density[a] (Jy ± mJy)	Observed Position (J2000.0) R.A.	Observed Position (J2000.0) Decl.	Offset[b] (arcsec)
2001 Oct 15	2.46 ± 3.9	10 35 07.1	56 28 47	1.5
2002 Apr 7	2.39 ± 5.6	10 35 07.0	56 28 48	1.0
2002 Jun 24	2.08 ± 2.9	10 35 06.9	56 28 47	1.5
2002 Sep 21	2.33 ± 3.3	10 35 07.1	56 28 46	1.8
2003 Jun 13[c]	1.89 ± 1.6	10 35 07.0	56 28 47	0.0

Note.—Units of right ascension are hours, minutes, and seconds, and units of declination are degrees, arcminutes, and arcseconds.
[a] Note that the flux density is in janskys and error is in millijanksys. Errors are best-fit errors obtained from the AIPS task *jmfit*.
[b] Offsets are from the optical position of the sources given in NED.
[c] Note that this observation is at frequency 1280 MHz, whereas other observations are at 1390 MHz.

variations due to the bad weather and related causes and improved the images considerably. After imaging, all the subfields were combined into a single field using the AIPS task *flatn*. All data sets were corrected for the primary beam pattern of the antennas. Figure 1 shows the SN 1993J image on 2002 March 8 at the 243 MHz band. Figure 1 (*left*) shows the full field of view, which was imaged after dividing it into 25 subfields and subsequently recombining. The positions of the supernova, the parent galaxy M81, and the nearby starburst galaxy M82 are shown separately in the right panels. Table 1 gives the details of the observations and analysis of all the data sets at the GMRT observation epochs.

2.4. *Errors in the Flux Density Determination*

Apart from the noise in the map plane (rms $\propto [n(n-1)\Delta\nu\tau]^{-1/2}$, where n is the number of baselines, $\Delta\nu$ is the bandwidth of the observations, and τ is the integration time), there are other factors that contribute to the errors in the flux density determinations. These could be modulations due to interstellar scattering and scintillation, elevation-dependent errors, errors due to the bandwidth smearing, and errors due to the use of two-dimensional geometry in the imaging. The last two errors can be corrected for by following the procedure mentioned in § 2.3. Here we discuss mainly the interstellar scattering and scintillation effects and elevation-dependent errors that contribute to the uncertainty in the source flux density determination.

2.4.1. *Interstellar Scattering and Scintillation*

We calculated the effect of the interstellar scattering and scintillation in the supernova at all observed frequencies. Figure 1 of Walker (1998) suggests that the transition frequency ν_0 (the frequency corresponding to unit scattering strength)[2] for the position of SN 1993J ($l = 142\overset{\circ}{.}15$, $b = 40\overset{\circ}{.}92$) is 8 GHz. Since all the frequencies of our observations are less than the

[2] Scattering strength is unity when the phase change across the first Fresnel zone introduced by interstellar medium inhomogeneities is of the order of half a radian (Walker 1998).

TABLE 4
Details of the GMRT Observations of Phase Calibrator 0834+555

Date of Observation	Frequency (MHz)	Flux Density[a] (Jy ± mJy)	Observed Position (J2000.0) R.A.	Observed Position (J2000.0) Decl.	Offset[b] (arcsec)
2000 Nov 8	1420	8.80 ± 8.5	08 34 54.9	55 34 24	3.0
2000 Dec 16	1420	8.75 ± 6.6	08 34 55.0	55 34 14	7.1
2001 Jun 2	1390	8.71 ± 4.2	08 34 52.2	55 34 38	43.9
2001 Mar 24	610	8.47 ± 17.8	08 34 54.9	55 34 34	13.0
2001 Aug 24	610	8.18 ± 12.6	08 34 55.1	55 34 20	1.8
2001 Dec 30	610	8.74 ± 13.8	08 34 54.9	55 34 22	1.0
2002 Mar 8	610	8.23 ± 12.5	08 34 54.9	55 34 21	0.0
2002 May 19	610	8.44 ± 20.0	08 34 54.9	55 34 21	0.0
2002 Sep 16	610	8.50 ± 11.3	08 34 54.9	55 34 21	0.0
2003 Jun 17	610	8.14 ± 15.7	08 34 54.9	55 34 21	0.0
2001 Jul 5	325	8.96 ± 26.6	08 34 55.0	55 34 24	3.4
2002 Mar 7	325	8.76 ± 6.8	08 34 55.0	55 34 22	1.8
2002 Aug 16	325	9.06 ± 31.9	08 34 54.9	55 34 21	0.0
2001 Dec 31	243	8.77 ± 46.8	08 34 54.9	55 34 21	0.0
2002 Mar 8	243	8.20 ± 36.6	08 34 55.0	55 34 24	3.4
2002 Sep 16	243	9.02 ± 43.8	08 34 55.0	55 34 20	1.8
2003 Jun 17	243	8.25 ± 44.7	08 34 54.9	55 34 21	0.0

Note.—Units of right ascension are hours, minutes, and seconds, and units of declination are degrees, arcminutes, and arcseconds.
[a] Note that the flux is in janskys and error is in millijanskys. Errors are best-fit errors obtained from AIPS task *jmfit*.
[b] Offsets are from the optical position of the sources given in NED.

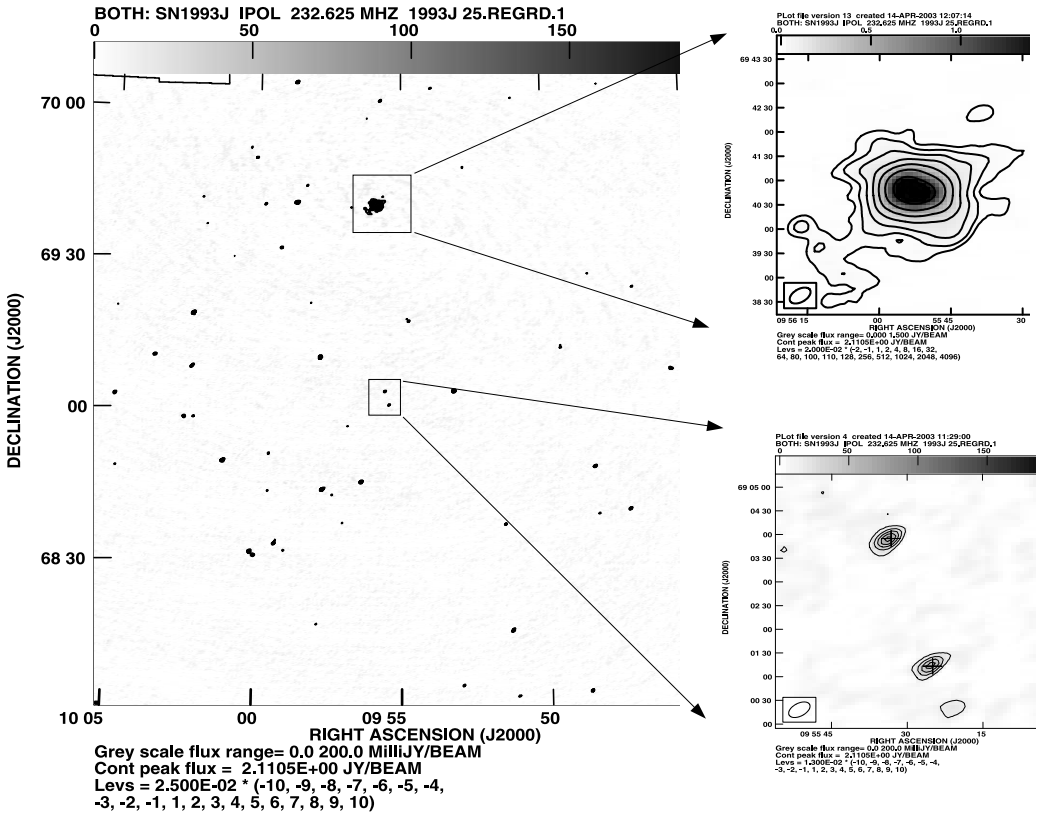

FIG. 1.—*Left*, GMRT contour map of the field of view of SN 1993J in the 243 MHz band (observed on 2002 March 8) *top right*, M82; *bottom right*, parent galactic center M81 (*upper contours*) and SN 1993J (*lower contours*).

transition frequency, the target should be in the strong scattering regime. Figure 3 of Kulkarni et al. (1998) suggests that strong short-time diffractive scintillation occurs in the very early stages of the supernova, when its size is still very small. Their figure suggests that SN 1993J is in the refractive interstellar scintillation (RISS) regime at the present epoch. During the GMRT observations epoch, i.e., around day 3000 after the SN 1993J explosion, we take the size of the supernova to be $\theta_s \sim 5000$ μas (Bartel et al. 2002). The Fresnel size of the source is $\theta_r \propto (\nu_0/\nu)^{11/5}$ (Walker 1998). We thus find that the supernova is in the point-source limit only for 243 MHz, since for this frequency $\theta_s \leq \theta_r$ ($\theta_r \sim 9000$ μas), and is in the extended source limit ($\theta_s \geq \theta_r$) for all other frequencies ($\theta_r \sim 4500$ μas at 325 MHz, $\sim$1150 μas at 610 MHz, and $\sim$200 μas at 1420 MHz). For RISS in the point-source regime, the modulation index m_p (rms fractional flux variation) and the refractive scintillation timescale t_r are

$$m_p = (\nu/\nu_0)^{17/30}, \quad t_r(\mathrm{hr}) \propto (\nu_0/\nu)^{11/5},$$

respectively. In the extended-source regime, these factors are further modified. The modulation index is reduced by $(\theta_r/\theta_s)^{7/6}$, and the refractive timescale is increased by θ_s/θ_r (Walker 1998). We calculate that at 243 MHz, the modulation index is 13.8%, whereas the timescale of modulation is $\sim$180 days. The modulation index and the timescale of modulation at 325 MHz are 14.7% and $\sim$100 days, respectively. At the 610 MHz band, the modulation index is 4.2%, whereas the timescale of variation is 100 days. At 1420 MHz, the modulation index (0.8%) is negligible, and the timescale of variation is 100 days. We therefore conclude that interstellar scintillations and scattering are not likely to significantly modulate our flux densities on short timescales (such as $\sim$2 months).

2.4.2. *Elevation-dependent Errors*

At high frequencies, there are noticeable changes in the antenna gains with the change of elevation angle with time. Atmospheric opacity also introduces an elevation dependence on the observed visibility amplitudes. By calibrating the target source with a nearby calibrator, these variations can be accounted for to a large extent. However, if the primary flux calibrator is observed at an elevation different from that of the secondary gain and phase calibrator, it may lead to significant errors. Proper calibration of the flux densities at high frequencies requires the knowledge of a gain curve for the antennas, as well as the atmospheric opacity. For low frequencies such as 610, 325, and 243 MHz, elevation-dependent errors are quite negligible for most of the sources. At the 1420 MHz wave band, elevation-dependent errors may affect the observations. However, SN 1993J is at such a high declination (69°) that the data are unlikely to be severely affected by such errors. We ran the AIPS task *elint* to determine the elevation-dependent errors for the phase calibrators. We find that the errors are $\sim$5%–6% in the 1420 MHz band and $\sim$2%–4% in the 610, 325, and 243 MHz bands. However, the actual errors may be a little larger than this because the program source (SN 1993J) is another 15°–20° away from the phase calibrators.

2.4.3. *Calibration Errors*

In some of the observations, we had more than one flux calibrator. In such instances we could estimate the calibration errors in the GMRT bands by using the following procedure:

We assumed one flux calibrator (e.g., A) to be the absolute calibrator and calculated the flux density of the absolute calibrator using the Baars formulation. We then calibrated another flux calibrator (e.g., B) with respect to the absolute calibrator (A) and obtained the flux density of calibrator B with respect to A [$B(A)$]. Since we already had the flux density of flux calibrator B using the Baars formulation [B(Baars)], the difference of $B(A)$ and B(Baars), $|B(A) - B(\text{Baars})|$, is an indicator of the calibration errors in GMRT. We found that the calibration errors for the 1420, 610, 325, and 243 MHz bands are in the range of 3%–4%, 4%–6%, 5%–7%, and 5%–8%, respectively.

To incorporate all the errors discussed above, we have used the following formula to quote the errors in the flux density determination for our GMRT data sets:

$$\sqrt{(\text{map rms})^2 + (10\% \text{ of peak flux of SN})^2}.$$

The overall error of 10% of the peak flux density at all the frequencies takes into account any possible systematic error in the GMRT measurements, including the small errors due to the antennas' elevation dependence. This 10% is close to the actual errors in the low-frequency 240 and 325 MHz bands but is an upper limit for the higher frequencies of 1420 and 610 MHz, where the overall errors are more likely to be 7%–8%.

3. RESULTS AND INTERPRETATION

3.1. *Light Curves of SN 1993J*

In Figure 2 we show the light curves of SN 1993J in all the frequency bands reported in Table 1. We interpret here the gross features of these light curves. The light curves in the 1420 and 610 MHz bands show a decline with time. This is the expected behavior of a supernova in the optically thin part of the light curve, where the decline is a power law in time. There appears to be a hint of a jump in the light curve somewhere between 3123 and 3296 days in the 1420 MHz frequency band. If the variation is real, the most natural explanation of this variation could be the inhomogeneity in the CSM or a nonuniform magnetic field in the plasma. Bartel et al. (2002) also found a sudden jump in the 8.4 GHz light curve around day 2000. We consider it likely that the jump in the 1420 MHz light curve referred to here is real, and since the evolutions of supernova light curves repeat at lower frequencies at later times, the earlier jump in the 8.4 GHz light curve should be seen later in the 1.4 GHz band. However, in view of the uncertainties in the flux determinations, this conclusion is not robust at present. Future observations at lower frequencies will be a good check of the possible jumps in the supernova light curve, for if the jumps are real, then they will show up at lower frequencies at later epochs. The 325 MHz light curve also shows a declining trend, although in a less rapid manner than for the light curves at higher frequencies. It is likely that the supernova has just become optically thin in the 325 MHz band, and hence the decline is much slower. However, the 235 MHz light curve is more or less flat, as is expected when the light curve is going through a peak. The shapes of the spectral fits in radio also suggest this (see § 3.2) and indicate that the light curve of the SN 1993J may remain flat at the 235 MHz band for the next few years.

Because of the small number of data points, we did not attempt detailed fits of the light curves with various models. However, we attempted to compare our data points with the already existing models. We used a model of synchrotron radio emission with FFA (Weiler et al. 2002). The FFA model for the SN 1993J light curves (Weiler et al. 2002) gives

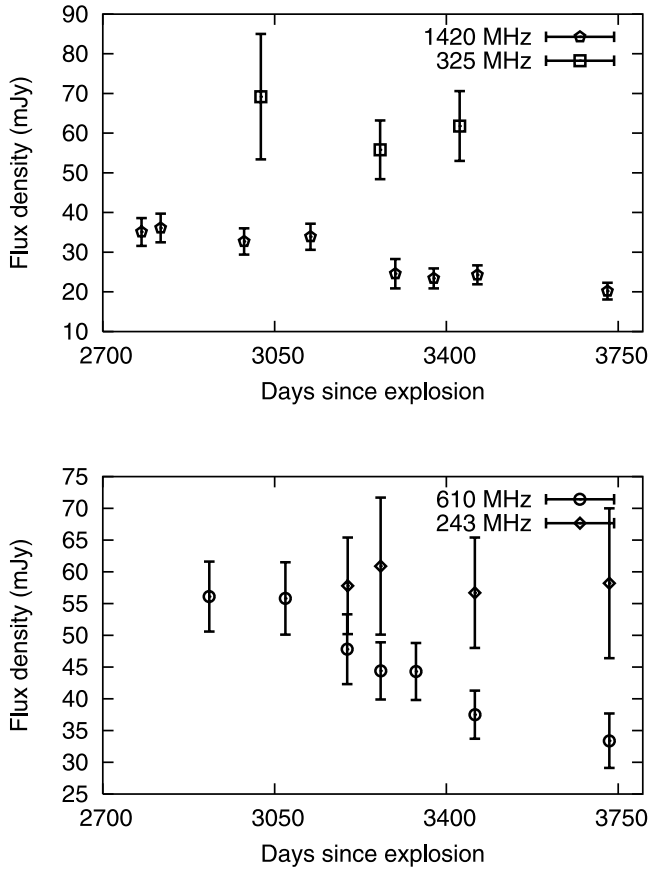

FIG. 2.—Light curves of SN 1993J at the 1420 and 325 MHz bands (*top*) and the 610 and 235 MHz bands (*bottom*), observed with the GMRT.

$$F_\nu(\text{mJy}) = K_1 \left(\frac{\nu}{5\ \text{GHz}}\right)^{\alpha} \left(\frac{t - t_0}{1\ \text{day}}\right)^{\beta} e^{-\tau} \left(1 - e^{-\tau'}\right) (\tau')^{-1}, \quad (1)$$

where

$$\tau = K_2 \left(\frac{\nu}{5\ \text{GHz}}\right)^{-2.1} \left(\frac{t - t_0}{1\ \text{day}}\right)^{\delta}, \quad (2)$$

$$\tau' = K_3 \left(\frac{\nu}{5\ \text{GHz}}\right)^{-2.1} \left(\frac{t - t_0}{1\ \text{day}}\right)^{\delta'}. \quad (3)$$

Here K_1, K_2, and K_3 are free parameters corresponding to the flux density and uniform and nonuniform external absorption, respectively, at 5 GHz, 1 day after the explosion date t_0. The free parameters α and β are the emission index and time index, respectively. The parameters δ and δ' describe the time dependence of the optical depths for the uniform and nonuniform CSM. The best-fit parameter values for SN 1993J (Weiler et al. 2002) are $K_1 = 1.86 \times 10^4$, $\alpha = -1.07$, $\beta = -0.93$, $K_2 = 1.45 \times 10^3$, $\delta = -2.02$, $K_3 = 6.31 \times 10^4$, and $\delta' = -2.14$. This model was fitted for high-frequency VLA observations in the 22.5–1.4 GHz frequency bands. We extrapolate this model to the 1420, 610, 325, and 243 MHz frequencies at the GMRT observation epochs with the above parameters. Figure 3 shows these extrapolated light curves for the supernova at 1420, 610, 325, and 243 MHz and our corresponding GMRT data points at the respective frequencies.

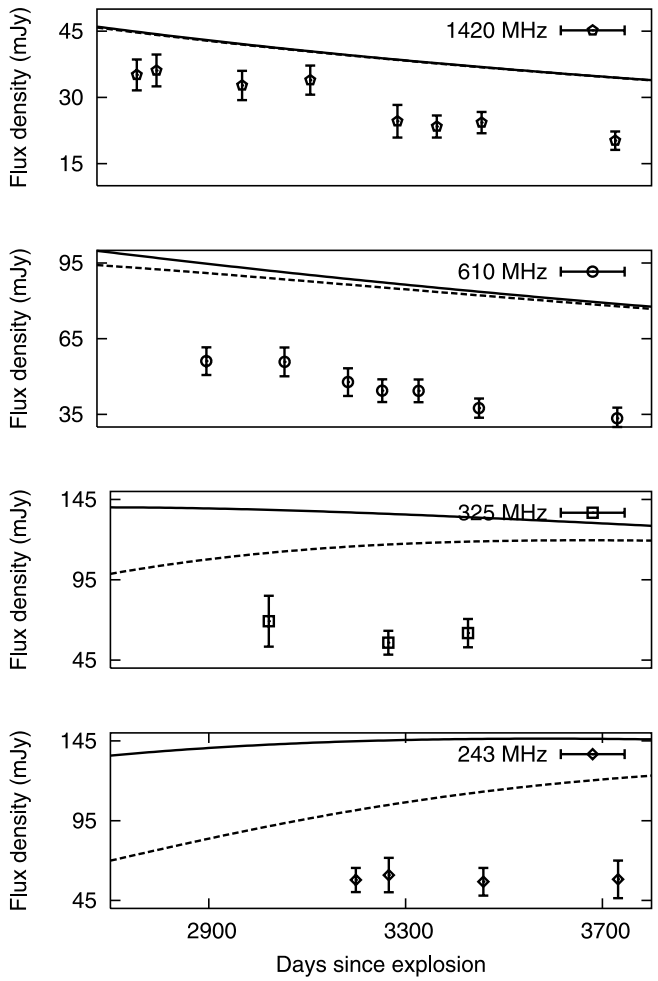

FIG. 3.—Comparison of low-frequency data with the predictions of models obtained by fitting high-frequency fluxes of SN 1993J. The solid lines in all four plots are from the Weiler et al. (2002) model extrapolated to lower frequencies (see § 3.1). Dashed lines show the flux density plots after incorporating the SSA optical depth in the Weiler et al. free-free model.

It is evident that the free-free model described above overpredicts the flux densities at low frequencies. In fact, the lower the frequencies, the more significant is the departure from the standard free-free model. This indicates that the optical depths fitted using high-frequency data sets, simply extrapolated to low frequencies with the dependence $\tau \propto \nu^{-2.1}$, are not sufficient to account for the required absorption. One needs to incorporate some additional frequency-dependent opacity at low frequencies that can compensate for the difference between the model light curves and the actual data.

Since the extrapolation of the free-free model of Weiler et al. (2002) with the above parameters to low frequencies, for instance, 1420, 610, 325, and 243 MHz, tends to overpredict the flux density of the supernova, we incorporated an extra opacity due to SSA to check whether this brings the observed flux points into consistency. The SSA absorption coefficient is given as (Pacholczyk 1970)

$$\kappa_{\rm SSA} = \frac{\sqrt{3}e^3}{8\pi m}\left(\frac{3e}{2\pi m^3 c^5}\right)^{\gamma/2} cB^{(\gamma+2)/2} \times \Gamma\left(\frac{3\gamma+2}{12}\right)\Gamma\left(\frac{3\gamma+22}{12}\right)\nu^{-(\gamma+4)/2}. \quad (4)$$

We assumed the shell size (from which the radio emission comes) to be 20% (Bartel et al. 2002) of the supernova size and took the SSA optical depth to be $\tau_{\rm SSA} = \kappa_{\rm SSA} R/5$, with $R \propto t^{0.781}$ (Bartel et al. 2002). To incorporate the absorption due to SSA, we add the optical depth $\tau_{\rm SSA}$ to equation (3) and obtain

$$\tau_{\rm int} = \tau' + \tau_{\rm SSA}, \quad (5)$$

and the flux density of the supernova including the SSA absorption is

$$F_\nu^{\rm SSA}({\rm mJy}) = K_1\left(\frac{\nu}{5\ {\rm GHz}}\right)^{\alpha}\left(\frac{t-t_0}{1\ {\rm day}}\right)^{\beta}\left(\frac{1-e^{-\tau_{\rm int}}}{\tau_{\rm int}}\right), \quad (6)$$

where the last bracketed term is the attenuation due to the total internal absorption including SSA absorption. Figure 3 shows the light curves at 1420, 610, 325, and 243 MHz after incorporating the extra SSA opacity. We note that even after adding this extra opacity in the existing free-free model, the total optical depth is not sufficient to reproduce the observed flux density. The medium is more opaque to radio emission at the lower frequencies.

3.2. *Spectra of SN 1993J*

On five different occasions we collected simultaneous or near-simultaneous spectra of SN 1993J by making flux density measurements at multiple frequencies separated by about a month or so. Since the supernova is ~10 yr old, we do not expect its flux density to change by a significant amount in the month's gap between the two flux density measurements. For example, taking the flux density dependence on time t to be $F \propto t^{-0.93}$ (Weiler et al. 2002), we find that the flux density of the supernova will change by only 2% in 75 days at such late epochs. This is well within the uncertainties of the flux measurements. We also saw in § 3.1 that the timescale of the flux density variation due to RISS is 6 and 3 months at lower and higher frequencies, respectively, and hence RISS will not contribute significantly to the flux density variations within a month's time gap. Therefore, we can use the observations separated by roughly a month to obtain a near-simultaneous spectrum of the supernova. Table 5 gives the details of the observations used to obtain the spectra with GMRT at five different epochs.

With so few data points in the spectra, it is difficult to distinguish between the SSA model and the FFA mechanism as the dominant underlying cause of absorption. We use an SSA radio emission model to fit our data sets (see Chevalier 1998; Pacholczyk 1970), which we justify in § 3.3:

$$f_\nu^{\rm SSA} = \frac{\pi R^2}{D^2}\frac{c_5}{c_6}B^{-1/2}\left(\frac{\nu}{2c_1}\right)^{5/2}[1-g(\nu,\ \gamma)], \quad (7)$$

where

$$g(\nu,\ \gamma) = \exp\left[-\left(\frac{\nu}{2c_1}\right)^{-(\gamma+4)/2}\left(\frac{4fRc_6N_0B^{(\gamma+2)/2}}{3}\right)\right], \quad (8)$$

$$N_0 = \frac{aB^2(\gamma-2)E_l^{\gamma-2}}{8\pi}. \quad (9)$$

TABLE 5
DETAILS OF THE NEAR-SIMULTANEOUS SPECTRA OF SN 1993J

Date of Observation	Days after Explosion	Frequency Band (MHz)	Flux Density (mJy)	rms (mJy)
2001 Jul 5	3022	325	69.2 ± 15.8	2.5
2001 Aug 24	3072	610	55.8 ± 5.7	0.4
2001 Jun 2	2988	1390	32.7 ± 3.3	0.2
2001 Dec 31	3199	243	57.8 ± 7.6	2.5
2001 Dec 30	3198	610	47.8 ± 5.5	1.9
2001 Oct 15	3123	1390	33.9 ± 3.5	0.3
2002 Jan 13[a]	3212	1460	31.44 ± 4.28	2.9
2002 Jan 13[a]	3212	4885	15 ± 0.77	0.19
2002 Jan 13[a]	3212	8440	7.88 ± 0.46	0.24
2002 Jan 13[a]	3212	14965	4.49 ± 0.48	0.34
2002 Jan 13[a]	3212	22485	2.50 ± 0.28	0.13
2002 Mar 8	3266	243	60.9 ± 10.8	4.1
2002 Mar 7	3265	325	56.2 ± 7.4	1.9
2002 Mar 8	3266	610	44.4 ± 4.5	0.3
2002 Apr 7	3296	1390	24.6 ± 3.7	1.0
2002 Sep 16	3458	243	56.7 ± 8.7	4.0
2002 Sep 16	3458	610	37.5 ± 3.8	0.4
2002 Sep 21	3463	1390	24.2 ± 2.4	0.2
2003 Jun 17	3732	243	58.2 ± 11.8	5.4
2003 Jun 17	3732	610	33.4 ± 4.3	0.8
2003 Jun 13	3728	1280	20.2 ± 2.1	0.2

[a] VLA data, courtesy of K. Weiler and collaboration.

The above flux density expression can be reduced to the following in the optically thin limit:

$$f_\nu^{\rm SSA}|_{\tau\le 1} = \frac{4\pi f R^3}{3D^2} c_5 N_0 B^{(\gamma+1)/2} \left(\frac{\nu}{2c_1}\right)^{-(\gamma-1)/2}; \quad (10)$$

in the optically thick limit,

$$f_\nu^{\rm SSA}|_{\tau\ge 1} = \frac{\pi R^2}{D^2}\frac{c_5}{c_6} B^{-1/2} \left(\frac{\nu}{2c_1}\right)^{5/2}. \quad (11)$$

Here R is the radius of the supernova, D is the distance to the supernova, f is the filling factor (which we took to be 0.5 for our purpose; Chevalier 1998), γ is the electron spectral index, which depends on the emission spectral index α as $\gamma = 2\alpha + 1$, N_0 is the normalization constant in the power-law distribution of electrons, $N(E) = N_0 E^{-\gamma}$ (Chevalier 1998), a is the equipartition factor ($a = U_{\rm rel}/U_B$, where $U_{\rm rel}$ is the relativistic electron energy density and U_B is the magnetic energy density), and E_l is the electron rest mass energy ($E_l = 0.51$ MeV). The (constant) parameters c_1, c_5, and c_6 are defined in Pacholczyk (1970); c_5 and c_6 are functions of the electron spectral index γ and are tabulated in Table 7 of Appendix 2 in Pacholczyk (1970). They are

$$c_1 = \frac{3e}{4\pi m^3 c^5} = 6.27\times 10^{18} \text{ cgs units},$$

$$c_5 = \frac{\sqrt{3}e^3}{16\pi}\frac{e^3}{mc^2}\left(\frac{\gamma+7/3}{\gamma+1}\right)\Gamma\left(\frac{3\gamma-1}{12}\right)\Gamma\left(\frac{3\gamma+7}{12}\right),$$

$$c_6 = \frac{\sqrt{3}\pi}{72} em^5 c^{10}\left(\gamma+\frac{10}{3}\right)\Gamma\left(\frac{3\gamma+2}{12}\right)\Gamma\left(\frac{3\gamma+10}{12}\right).$$

The parameters R, B, and α or γ are the three free parameters for fitting a model to the observed spectrum.

On day 3200, we combined the GMRT low-frequency spectrum with that of high-frequency VLA data (kindly provided by K. Weiler, C. Stockdale, and their collaboration) and fitted the SSA model (Fig. 4, *solid line*). We found that the spectrum at high frequency is best fitted by a broken power law with a break around 4 GHz, which we interpret as being due to synchrotron cooling. SN 1993J is the first such young supernova in which a synchrotron cooling break in the radio frequency region is seen. The observational signature of the synchrotron cooling break directly leads to the determination of the magnetic field in the plasma. This is the most direct determination of the magnetic field in the shocked plasma (Chandra et al. 2004a), since the age of the source is known.

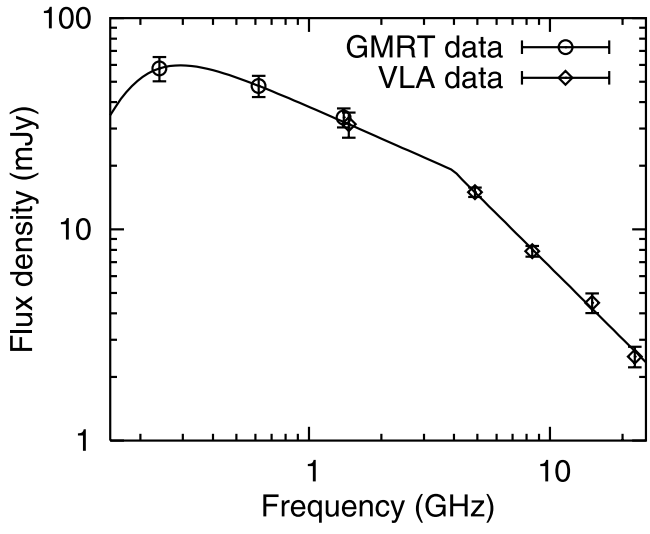

FIG. 4.—GMRT plus VLA combined spectrum on day 3200. The solid line shows the best-fit SSA model. The spectrum shows a break at 4 GHz, with a steepening in the spectral index by 0.62 (Chandra et al. 2004a).

TABLE 6
BEST-FIT PARAMETERS OF SSA FITS TO THE GMRT SPECTRA

DAYS AFTER EXPLOSION	SPECTRAL INDEX α[a]	SSA BEST FIT	
		B (G)	R ($\times 10^{17}$ cm)
3000	0.65 ± 0.17	0.28 ± 0.12	2.71 ± 0.43
3200	0.51 ± 0.21[b]	0.43 ± 0.19[c]	3.26 ± 0.41
3266	0.71 ± 0.22	0.24 ± 0.11	3.11 ± 0.58
3460	0.53 ± 0.17	0.19 ± 0.09	4.10 ± 0.50
3730	0.68 ± 0.21	0.15 ± 0.07	4.83 ± 0.69

[a] Values for α are calculated manually from the assumed optically thin part of the spectrum between 610 and 1420 MHz.
[b] Spectral index α *before* the break in the spectrum.
[c] This determination of B is from the best-fit SSA model. The magnetic field using the synchrotron cooling break is 0.33 G. Both values match within error bars.

The lifetime of the relativistic electrons undergoing synchrotron loss is given as

$$t = \tau = E/\left[-(dE/dt)_{\rm sync}\right] = 1.43\times10^{12}B^{-3/2}\nu_{\rm break}^{-1/2}\ {\rm s}. \quad (12)$$

Here we use $B_\perp^2 = (B\sin\theta)^2 = (2/3)B^2$. However, we also include energy loss/gain due to the adiabatic expansion and the diffusive shock acceleration (Fermi acceleration) along with the synchrotron energy-loss term, for the supernova is young, and these process are likely to be important (see Chandra et al. 2004a). Hence, the lifetime of electrons for the cumulative energy-loss rate is

$$\tau = \frac{E}{(dE/dt)_{\rm total}} = \frac{E}{(R^2t^{-2}/20\kappa_\perp)E - bB^2E^2 - t^{-1}E}, \quad (13)$$

where the second term in the denominator is the synchrotron loss term, with $b = 1.58\times10^{-3}$, the first term is the energy gain due to diffusive shock acceleration, and the third term is the adiabatic expansion loss term. Using $\nu_{\rm break} = 5.12\times10^{18}\ BE_{\rm break}^2$ Hz (Pacholczyk 1970) in the above equation, we found the magnetic field implied by the lifetime argument to be $B = 330$ mG. On the other hand, from the best fit with SSA, the magnetic field under equipartition assumption is $B_{\rm eq} = 38 \pm 17$ mG. Comparison of the magnetic field obtained from the lifetime argument with that obtained from the SSA model best fit (assuming equipartition) determines the value of the equipartition fraction between the relativistic energy of the particles and the magnetic field energy. The equipartition fraction $a = U_{\rm rel}/U_{\rm mag}$ varies with the magnetic field B as $a = (B/B_{\rm eq})^{-(2\gamma+13)/4}$ (Chevalier 1998). Therefore, the fraction a ranges between 8.5×10^{-6} and 4.0×10^{-4} with a central value of $a = 1.0\times10^{-4}$ (corresponding to $B_{\rm eq} = 38$ mG) on day 3200. The plasma is thus dominated by the magnetic field, whose energy density far exceeds that of the relativisitic particles. As Chevalier (1998) has argued, it is likely that this high magnetic field is the result of an amplification process in the interaction region and is not merely the effect of shock compression of the magnetic field in the wind by the relevant compression ratio. See Chandra et al. (2004a) for a detailed study of the combined spectrum (GMRT and VLA) with the break.

The above analysis shows that if we were to fit the SSA model under the assumption of equipartition, we would end up seriously underpredicting the magnetic field as roughly an order of magnitude lower than the actual field. The relativistic plasma is far from equipartition and is strongly dominated by the magnetic energy density. We assume that the equipartition fraction, as determined above on day 3200, does not change with time. Using this fraction, we can fit the SSA model to our subsequent GMRT spectra and determine the most probable values of the free parameters, e.g., R, B, and α, in the SSA model. Since we have very few data points for the spectra, we cannot determine all three parameters. Therefore, we separately calculated the value of the spectral index α using the optically thin part of the spectrum ($F_\nu \propto \nu^{-\alpha}$) between the frequencies of 610 and 1420 MHz. The errors in the values of the spectral indices reflect the errors in the flux densities at a given frequency. The size of the supernova and the magnetic field were used thereafter as free parameters in the SSA fits to the spectra. The best-fit magnetic field and the size of the supernova thus obtained and reported in Table 6 *are not under the assumption of equipartition* of relativistic particles and fields. The errors in B and R are large because of a large range in the equipartition fraction a ($B \propto a^{-4/(2\gamma+13)}$; $R \propto a^{-1/(2\gamma+13)}$). Figure 5 shows the GMRT spectra at days 3000, 3200, 3266, 3460, and 3730 after the explosion. The spectrum currently appears to peak around 235 MHz because of the flattening of the light curves at these frequencies and is gradually shifting to lower frequencies. Data in the still lower frequency bands ($<$235 MHz) may constrain the peak more tightly. We estimate below some of the physical parameters of the supernova based on the spectral fits and compare them with those determined by independent methods.

3.3. *Role of Synchrotron Self-Absorption at Spectral Turnover*

We fitted only the SSA model to the obtained spectra. However, we have also tried to fit the FFA model to the spectra. Since there are few data points in each spectrum, these models are not easily distinguished from each other by the data. However, the SSA model can be indirectly tested by comparing its predicted parameters against similar quantities measured entirely independently. For example, SN 1993J has been extensively studied using VLBI, and therefore the size of the supernova is known from these measurements. We also obtain the size of the supernova from the SSA model using the turnover in the spectra. Comparing the sizes obtained from these two independent methods therefore tests the SSA model. GMRT observations are only around day 3000 and later. To evaluate the SSA model at earlier epochs, we used VLA data available on the Internet[3] for days 65–250. We digitized the

[3] See http://rsd-www.nrl.navy.mil/7213/weiler/kwdata/93jdata.asc.

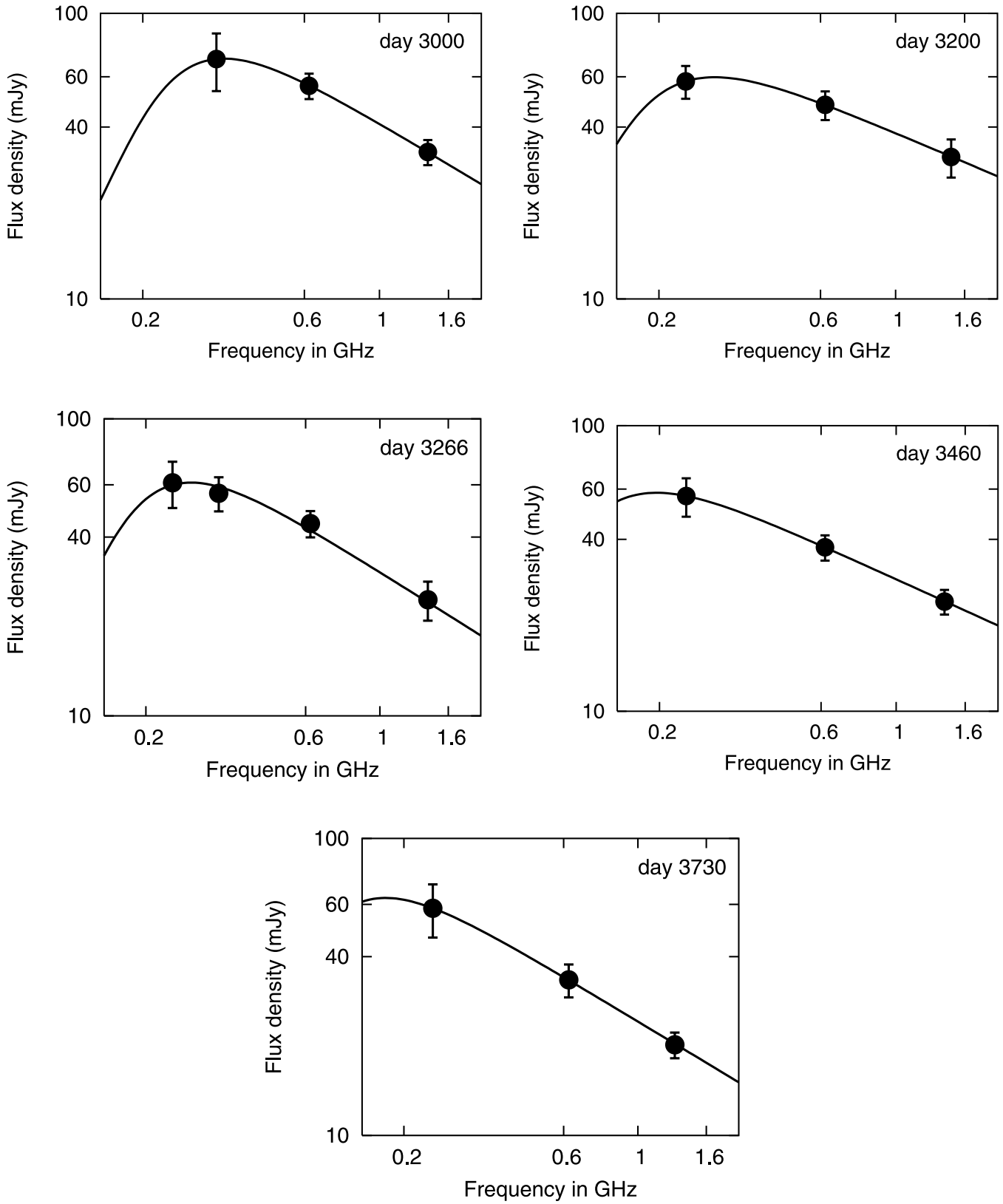

FIG. 5.—Best-fit GMRT spectra of SN 1993J on days ~3000, 3200, 3266, 3460, and 3730 after the explosion from top left in clockwise order. Solid lines show the SSA best-fit models (see Table 6 for details).

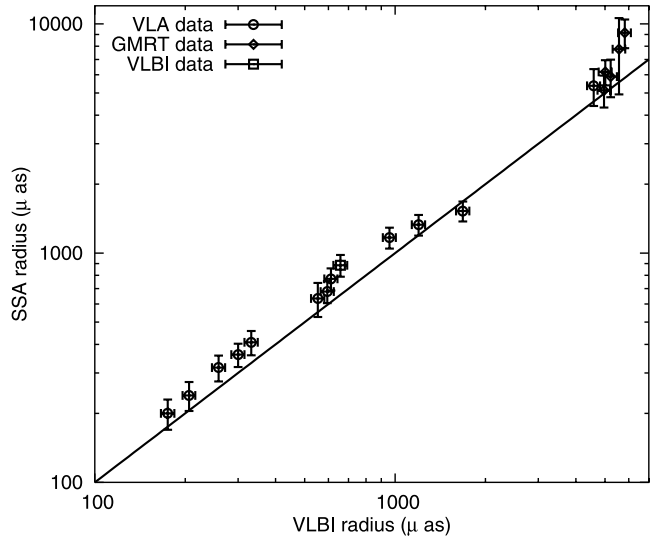

FIG. 6.—Size of SN 1993J from the SSA fit against the VLBI size. The straight line indicates the region where the SSA size equals the VLBI size of the supernova.

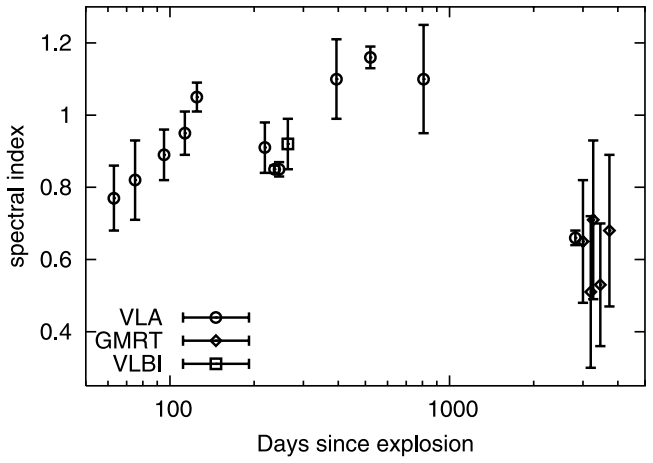

FIG. 7.—Evolution of the best-fit spectral index α with time. The spectral index changes from $\sim$1 to $\sim$0.6.

VLA data for days 400–800 from the available light curves (Van Dyk et al. 1994; Fransson & Bjornsson 1998). We also used the published data of Bartel et al. (2002) and Perez-Torres et al. (2002). We fitted the SSA model to the spectra at all these epochs using the equipartition fraction derived in Chandra et al. (2004a) and obtained the best-fit magnetic field and size of the supernova. We compared the best-fit size so obtained with that of the VLBI size of the supernova at various epochs obtained from Figure 6 of Bartel et al. (2002). Figure 6 shows the SSA size of the supernova plotted against the VLBI size of the supernova. At late epochs beyond day 3000, no VLBI observations were available, so we extrapolated the earlier VLBI observations to obtain the sizes of the supernova at the relevant epochs, assuming the latest value of $m = 0.781$ in $R \propto t^m$ (Bartel et al. 2002). We note that the VLBI size of the supernova and the SSA model fit size from the peak of the spectrum are largely consistent at all epochs. If SSA were not the most important absorption mechanism, the supernova size determinations from the SSA model would have been smaller than the sizes obtained from VLBI (see Slysh 1990). Since the two are roughly consistent at all epochs, the conclusion that SSA is the dominant absorption mechanism determining the spectral turnover appears natural.

We notice that at late epochs beyond day 3400, the SSA radius is more than the extrapolated VLBI size. This could be due to the incorrect estimation of the extrapolated VLBI radius with the assumed m, at late epochs for which VLBI observations do not exist. In addition, uncertainties in the determination of the peak of the spectra due to the lack of very low frequency measurements may affect the accuracy of the SSA radius and associated parameters.

3.4. *Evolution of Spectral Index, Size, and Magnetic Field*

Figure 7 shows the evolution of the best-fit radio spectral index α. The spectral index evolves with time, and its value changes from $\alpha \sim 0.8$–1.0 (in the first few tens of days) to $\sim$0.6 (10 yr after the explosion). GMRT measurements of the spectral index have significant errors. This is because we have not fitted the spectral index with an SSA or FFA model, since we had very few frequency data points in the spectra. Instead we calculated the spectral index from the optically thin part of the GMRT spectra between the 610 and 1420 MHz frequency bands, using the relation $F_\nu \propto \nu^{-\alpha}$. Errors in the determination of α are partly due to the errors in the flux density measurements.

Figure 8 (*top*) shows the supernova size evolution with time. We also plot the indicative $R \propto t$ line in the figure. It is noted that at early epochs, the size evolution is consistent with $R \propto t$, i.e., supernova ejecta expansion is free expansion, while at late enough epochs, the expansion undergoes deceleration. These results are roughly consistent with those of Bartel et al. (2002) and Marcaide et al. (1997). We show the time variation of the radii determined from our SSA fits to GMRT spectra as an inset in Figure 8. Figure 8 (*bottom*) shows that the magnetic field decreases as the supernova ages. We also plot the indicative $B \propto t^{-1}$ line, and it suggests that within error bars, the magnetic field decreases according to $B \propto t^{-1}$ over the full time range. However, there seems to be a hint of flattening in the time development between $\sim$400 and 1300 days.

When SSA is the dominant absorption mechanism, it is not possible to estimate directly the circumstellar density, as is possible in the case of *dominant* external FFA, but in contrast, it is possible to estimate the radio supernova size if the radio peak flux is observed. This leads to the determination of the velocities of the outer parts of the supernova, which we find from the radii reported in Table 6 to be $v \approx 11,000$ km s^{-1} for $t \geq 3000$ days. As a comparison, note that the optical photosphere velocity decreased to the 7000–10,000 km s^{-1} range, even 10–30 days after the explosion (Ray et al. 1993).

3.5. *Mass-Loss Rate of the Progenitor Star*

Estimates of the mass-loss rate give crucial information about the progenitor star. Since typical ejecta velocities are $\sim$1000 times the wind velocities, information about mass-loss rate derived a few years after the explosion can trace the history of the progenitor star a few thousands of years before the explosion. This requires an assumption about the wind velocity for the mass-losing progenitor star when it exploded as a supernova. The wind velocities around red supergiant stars are $\sim$10 km s^{-1}, while those of blue supergiant stars are $\sim$1000 km s^{-1}. For SN 1993J, we assume in consonance with the data and models (see, e.g., Ray et al. 1993) that the progenitor star had an extended red supergiant–like envelope in its last stage of evolution; thus, we adopt a circumstellar wind velocity of

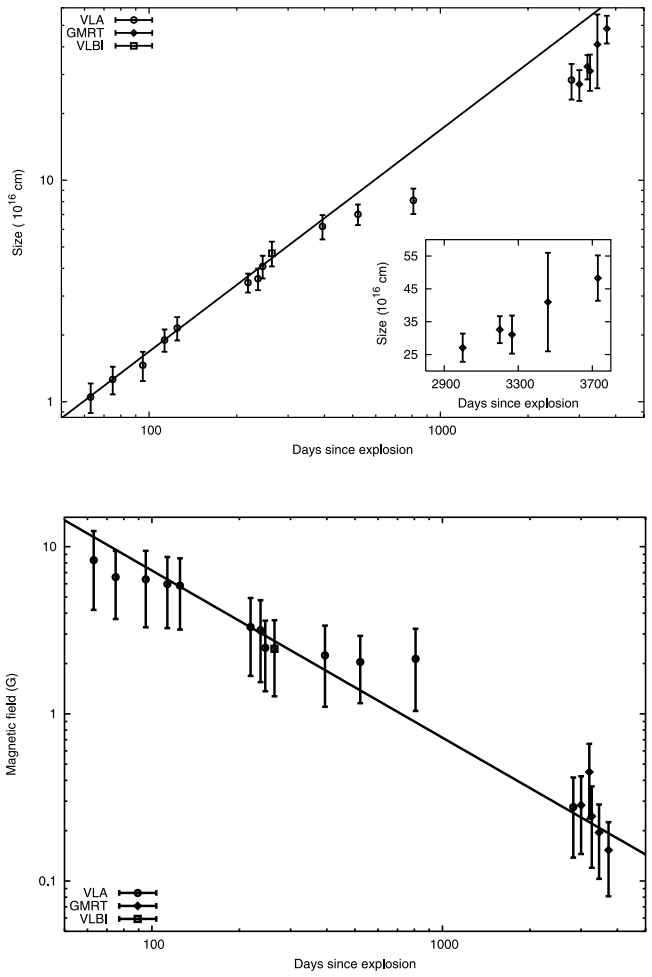

FIG. 8.—*Top*: Evolution of the size of the supernova with time. The straight line corresponds to $R \propto t$, i.e., free expansion. Initially, the expansion is free, but later it shows a deceleration. The inset shows the evolution of the size determined only from GMRT data (note the linear scales in time and radius here). *Bottom*: Evolution of the magnetic field in synchrotron-emitting plasma with time. The plot also shows the line corresponding to $B \propto t^{-1}$. The magnetic field evolution is roughly consistent with $B \propto t^{-1}$, although it shows some possible flattening around day 300–900.

10 km s^{-1}. We then determine the mass-loss rate using the best-fit parameters of SSA to the GMRT data (Table 6).

It is clear from § 3.2 that the magnetic energy density in SN 1993J considerably exceeds the relativistic particle energy density. However, these ratios are close to unity in some other supernovae, e.g., SN 2002ap (Bjornsson & Fransson 2004; Sutaria et al. 2003) and SN 1998bw (Kulkarni et al. 1998). Fransson & Bjornsson (1998) have also shown that there is a rough equipartition between the magnetic energy density and the thermal energy density in the postshock gas in SN 1993J. In turn, these are related to the ram pressure of the shock front. This leads to an estimate of the mass-loss rate from the supernova progenitor (Chevalier 1998) by relating the postshock magnetic energy density to the shock ram pressure, $B^2/8\pi = \zeta\rho_0 v_{\rm sh}^2$, where ζ is a numerical constant, ρ_0 is the postshock density, and $v_{\rm sh}$ is the shock velocity. For $\zeta \leq 1$, this gives a lower limit to the estimate of the mass-loss rate of

$$\dot{M} = \frac{6.6\times10^{-5}}{m^2\zeta}\left(\frac{B}{0.33\ \mathrm{G}}\right)^2\left(\frac{t}{3200\ \mathrm{days}}\right)^2\left(\frac{v_w}{10\ \mathrm{km\ s^{-1}}}\right) M_\odot\ \mathrm{yr}^{-1}. \quad (14)$$

TABLE 7

LOWER LIMITS TO THE MASS-LOSS RATES OF THE PROGENITOR OF SN 1993J FROM EQUATION (14) WITH $m = 0.781$

Days after Explosion	Years before Explosion[a]	Mass-Loss Rate ($10^{-5}\ M_\odot\ \mathrm{yr}^{-1}$)
3000	8219	6.8 ± 1.3
3200	8767	10.2 ± 3.6
3266	8948	5.9 ± 1.2
3460	9480	4.2 ± 0.9
3730	10219	3.01 ± 0.7

[a] Years before explosion is calculated by taking the ratio of the ejecta velocity to the wind velocity to be ~1000.

Here, $m = (n-3)/(n-2)$ is the deceleration index, where n is the ejecta density power law index. Although there are no VLBI measurements for the epoch of GMRT observations, we use the extrapolated value of the latest m obtained from VLBI, i.e., $m = 0.781$ (Bartel et al. 2002). We use the magnetic fields in the above equation that are determined from the spectral fits as given in Table 6. For $\zeta = 1$, the lower limit on the mass-loss rate can be calculated from equation (14). The values of the mass-loss rate for GMRT observations thus obtained are reported in Table 7. Figure 9 shows that the mass-loss rate (obtained from GMRT observations) appears to be decreasing slowly with a small slope of $1.8\times10^{-8}\ M_\odot\ \mathrm{yr}^{-2}$. (We assumed a constant ratio of the ejecta velocity and the wind velocity, $v_{\rm ej}/v_w \sim 1000$, to calculate the time before the explosion from the epoch after the explosion.) Note that the predicted mass-loss rate in Chevalier (1998) is constant, since it scales as B^2t^2, while his assumed time dependence is $B \propto 1/t$. However, GMRT data (from day 3000–3730, a relatively short range compared to the entire data span from the date of explosion) appear to indicate a slightly steeper dependence of B on $1/t$. Although the best-fit line to the mass-loss rate in Figure 9 in the narrow range of time before the explosion shows a small decrement, within the error bars of the GMRT measurements of B as seen in Figure 8, and also on the longer timescale after the explosion, our results are consistent with a constant mass-loss rate.

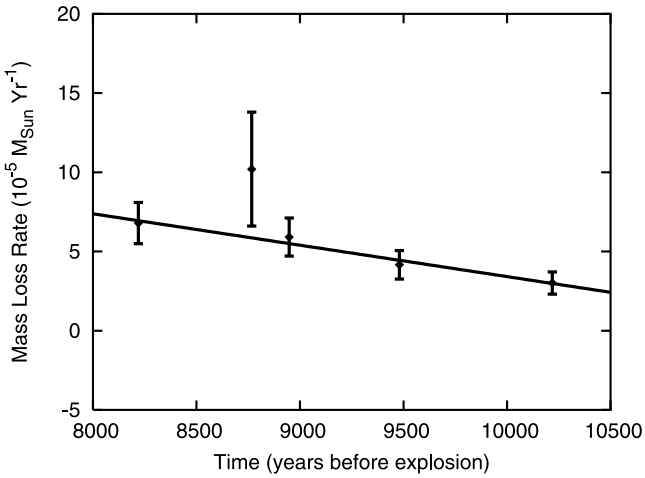

FIG. 9.—Evolution of the mass-loss rate of the presumed red supergiant progenitor of SN 1993J with time before the explosion of the star. The solid line represents the best fit with a slope of $1.8\times10^{-8}\ M_\odot\ \mathrm{yr}^{-2}$. Here the ratio of the ejecta velocity and wind velocity is taken to be ~1000 to compute the corresponding time before the explosion.

4. SUMMARY AND CONCLUSIONS

Even though SN 1993J has been one of the most well-observed targets since its explosion some 11 years ago, it continues to illuminate the physics of supernovae. SN 1993J is a unique supernova, for which the magnetic field and size are determined from model-independent measurements; the former from the synchrotron cooling break and the latter from VLBI measurements. These have been utilized here to test models and parameters that determine the radio emission from this supernova.

Because the radio emission from SN 1993J now peaks at frequencies lower than 235 MHz, it is necessary to observe it at low enough frequencies, at which it is still in the optically thick regime, to properly determine the turnover in the spectrum. Multifrequency spectra of SN 1993J ranging from the very low GMRT frequencies to very high VLA frequencies will thus be important observational inputs in the future. The synchrotron cooling break in the combined (VLA and GMRT) spectrum on day 3200 leads to the determination of the equipartition fraction between relativistic particle and magnetic energy densities (Chandra et al. 2004a). From the self-consistent analysis of early spectra of SN 1993J, Fransson & Bjornsson (1998) had interpreted a rough equipartition between the nonthermal ions, the magnetic field, and the thermal energy. We affirm that the relativistic particle energy density, however, is minuscule compared to the magnetic energy density in the radiating plasma.

The outer part of the supernova from which the radio emission originates is expanding at a speed of $\sim$11,000 km s^{-1} for $t \geq 3000$ days. This speed is small compared to those found in Type Ic supernovae such as SN 1998bw, SN 2002ap, and SN 2003dh (Ray et al. 2004), indicating that ordinary Type IIb supernovae such as SN 1993J have much less extreme properties than other core-collapse supernovae, some of which may produce gamma-ray bursts. Estimates of the mass lost from the progenitor star of SN 1993J derived from post-shock magnetic pressure, shock ram pressure, and the GMRT spectra indicate that the mass-loss rate remained roughly constant for 8000–10,000 yr before the explosion.

In our earlier paper (Chandra et al. 2004b), we had argued that the size of SN 1993J determined from the SSA fits is roughly half of that obtained from VLBI measurements. However, our earlier estimates of the size were based on the assumption of equipartition between magnetic and relativistic particle energy densities, since we did not have a direct handle on the equipartition fraction prior to the discovery of the synchrotron cooling break. In this paper we use the equipartition fraction directly determined from the synchrotron cooling break in the GMRT plus VLA spectrum on day 3200 (Chandra et al. 2004a) and thereby obtain the best-fit size of the supernova. We now find that our derived SSA sizes roughly match the VLBI sizes of the supernova at all epochs. We thus affirm that even if FFA had a significant contribution to the total absorption in the radio band, the peak in the spectrum is primarily determined by SSA. Slysh (1990) also had plotted the SSA sizes of a few supernovae against their VLBI sizes and found them to be consistent at all epochs. He then argued that SSA alone is responsible for the turnover in the spectra of supernovae. However, his results were based on the equipartition assumption between relativistic energy density and magnetic energy density. Our results on SN 1993J confirm the conclusion of Slysh (1990), namely, that SSA is the main absorptive process for the turnover, but unlike Slysh (1990), we do not assume an equipartition.

Light curves based on high-frequency FFA models extrapolated to low frequencies overpredict the flux densities at low frequencies. Some extra opacity is needed to incorporate the difference. We added extra opacity due to SSA, which also could not fully account for the required absorption. This suggests that the low-frequency opacity in SN 1993J is not a simple extrapolation of high-frequency opacity and that a hitherto unaccounted for absorption may be at work at low frequencies.

Bartel et al. (2002) have argued that the deceleration factor m ($R \propto t^m$) measured with the VLBI dropped from 0.92 to 0.78 around day 400, and then around day 1500, the decline of m stopped, and it increased to a value of 0.86. This trend was roughly mirrored in the light curves. They argue that the upturn in m could be due to the supernova ejecta hitting the reverse shock and exerting pressure in the forward direction. A nonuniform radial dependence of the CSM density can simultaneously provide a reasonable explanation of the nonsmooth evolution of the 1420 MHz flux between day 3150 and 3300. The flux density may increase if the supernova ejecta hits a clump in the CSM and decrease if the ejecta runs into a rarefied region. The enhanced emission due to the interaction with a clump may in effect lead to a flattening of the light curve rather than an actual rise, if the filling factor of the clumps is low near the radiosphere. A nonsmooth evolution of the radio luminosity can also be caused by inhomogeneities in the magnetic field in the interaction region, since synchrotron emission efficiency depends on the strength of the magnetic field. The synchrotron flux density has a dependence on magnetic field as $f_\nu^{\rm SSA}|_{\tau \geq 1} \propto B^{-1/2}$ in the optically thick part of the spectrum, and $f_\nu^{\rm SSA}|_{\tau \leq 1} \propto B^{(\gamma+1)/2}$ in the optically thin part. Therefore, the variation in the flux density with magnetic field is less significant in the optically thick regime than in the optically thin regime. Hence, jumps in the flux densities at high frequencies will be more evident than at lower frequencies. Because of the large errors of the measurements, one cannot ascertain whether the sudden jump in the light curve at 1420 MHz is real (although the same had been seen in 8.4 GHz light curves at earlier epochs by Bartel et al. [2002]). But if it is real, then it should be mirrored in low-frequency light curves at later epochs. Further observations at low frequencies will confirm it.

We thank Kurt Weiler for kindly providing the high-frequency flux densities from VLA observations on 2002 January 13. We thank the staff of the GMRT, which is run by the National Center for Radio Astrophysics of the Tata Institute of Fundamental Research (TIFR). We acknowledge the use of AIPS, which was developed by the staff of the National Radio Astronomical Observatory. We thank the anonymous referee for his/her detailed comments that helped us to improve the presentation of this work. P. C. is a recipient of the Sarojini Damodaran International Fellowship. This research is part of Tenth Five Year Plan project 10P-201 at TIFR, Mumbai.

REFERENCES

Baars, J. W. M., Genzel, R., Pauliny-Toth, I. I. K., & Witzel, A. 1977, A&A, 61, 99
Bartel, N., et al. 2002, ApJ, 581, 404
Bhatnagar, S. 2000, MNRAS, 317, 453
———. 2001, Ph.D. thesis, Univ. Pune
Bjornsson, C., & Fransson, C. 2004, ApJ, 605, 823
Chandra, P., Ray, A., & Bhatnagar, S. 2004a, ApJ, 604, L97
———. 2004b, in IAU Colloq. 192, Supernovae (10 Years of SN 1993J), ed. J. M. Marcaide & K. W. Weiler (Dordrecht: Springer), in press (astro-ph/0311418)
Chevalier, R. 1998, ApJ, 499, 810
Chevalier, R., & Fransson, C. 2003, in Supernovae and Gamma-Ray Bursters, ed. K. Weiler (New York: Springer), 171
Filippenko, A. V., Matheson, T., & Woosley, S. E. 1993, IAU Circ. 5787
Fransson, C., & Bjornsson, C. 1998, ApJ, 509, 861
Freedman, W. L., et al. 1994, ApJ, 427, 628
Höflich, P., Langer, N., & Duschinger, M. 1993, A&A, 275, L29
Kulkarni, S. R., et al. 1998, Nature, 395, 663
Marcaide, J. M., et al. 1997, ApJ, 486, L31
Maund, J. R., Smartt, S. J., Kudritzki, R. P., Podsiadlowski, P., & Gilmore, G. F. 2004, Nature, 427, 129
Nomoto, K., Suzuki, T., Shigeyama, T., Kumagai, S., Yamaoka, H., & Saio, H. 1993, Nature, 364, 507
Pacholczyk, A. G. 1970, Radio Astrophysics: Nonthermal Processes in Galactic and Extragalactic Sources (San Francisco: Freeman)
Perez-Torres, M. A., Alberdi, A., & Marcaide, J. M. 2002, A&A, 394, 71
Podsiadlowski, P. H., Hsu, J. J. L., Joss, P. C., & Ross, R. R. 1993, Nature, 364, 509
Ray, A., Chandra, P., Sutaria, F. K., & Bhatnagar, S. 2004, in IAU Colloq. 192, Supernovae (10 Years of SN 1993J), ed. J. M. Marcaide & K. W. Weiler (Dordrecht: Springer), in press (astro-ph/0311419)
Ray, A., Singh, K. P., & Sutaria, F. K. 1993, J. Astrophys. Astron., 14, 53
Ripero, J., Garcia, F., & Rodriguez, D. 1993, IAU Circ. 5731
Slysh, V. I. 1990, Soviet Astron. Lett., 16, 339
Sutaria, F. K., Chandra, P., Bhatnagar, S. & Ray, A. 2003, A&A, 397, 1011
Swartz, D. A., Clocchiatti, A., Benjamin, R., Lester, D. F., & Wheeler, J. C. 1993, Nature, 365, 232
Utrobin, V. 1994, A&A, 281, L89
Van Dyk, S. D., Garnavich, P. M., Filippenko, A. V., Höflich, P., Kirshner, R. P., Kurucz, R. L., & Challis, P. 2002, PASP, 114, 1322
Van Dyk, S. D., Weiler, K. W., Sramek, R. A., Rupen, R. P., & Panagia, N. 1994, ApJ, 432, L115
Walker, M. A. 1998, MNRAS, 294, 307
Weiler, K. W., Panagia, N., Montes, J. M., & Sramek, R. A. 2002, ARA&A, 40, 387
Weiler, K. W., Sramek, R. A., Rupen, M. P., & Panagia, N. 1993, IAU Circ. 5752
Weiler, K. W., Van Dyk, S. D., Discenna, J. L., Panagia, N., & Sramek, R. A. 1991, ApJ, 380, 161
Woosley, S. E., Eastman, R. G., Weaver, T. A., & Pinto, P. A. 1994, ApJ, 429, 300
Zimmermann, H.-U., et al. 1993a, IAU Circ. 5748
———. 1993b, IAU Circ. 5750